ACS OMEGA

Article

Cite This: ACS Omega 2019, 4, 6312−6323

http://pubs.acs.org/journal/acsodf

# Toward High Power Generating Piezoelectric Nanofibers: Influence of Particle Size and Surface Electrostatic Interaction of Ce−$Fe_2O_3$ and Ce−$Co_3O_4$ on PVDF

Hemalatha Parangusan,[†] Deepalekshmi Ponnamma,*[,†] and Mariam Al Ali AlMaadeed[‡]

[†]Center for Advanced Materials, Qatar University, P.O. Box 2713, Doha, Qatar

[‡]Materials Science & Technology Program (MATS), College of Arts & Sciences, Qatar University, Doha 2713, Qatar

Supporting Information

**ABSTRACT:** Development of flexible piezoelectric nanogenerator (PENG) is a real challenge for the next-generation energy-harvesting applications. In this paper, we report highly flexible PENGs based on poly(vinylidene fluoride) (PVDF)/2 wt % Ce−$Fe_2O_3$ and PVDF/2 wt % Ce−$Co_3O_4$ nanocomposite fibers. The incorporation of magnetic Ce−$Fe_2O_3$ and Ce−$Co_3O_4$ greatly affects the structural properties of PVDF nanofibers, especially the polymeric $\beta$ and $\gamma$ phases. In addition, the new composites enhanced the interfacial compatibility through electrostatic filler−polymer interactions. Both PVDF/Ce−$Fe_2O_3$ and PVDF/Ce−$Co_3O_4$ nanofibers-based PENGs, respectively, produce peak-to-peak output voltages of 20 and 15 V, respectively, with the corresponding output currents of 0.010 and 0.005 $\mu A/cm^2$ under the force of 2.5 N. Enhanced output performance of the flexible nanogenerator is correlated with the electroactive polar phases generated within the PVDF, in the presence of the nanomaterials. The designed nanogenerators respond to human wrist movements with the highest output voltage of 0.15 V, for the PVDF/Ce−$Fe_2O_3$ when subjected to hand movements. The overall piezoelectric power generation is correlated with the nanoparticle size and the existing filler−polymer and ion−dipole interactions.

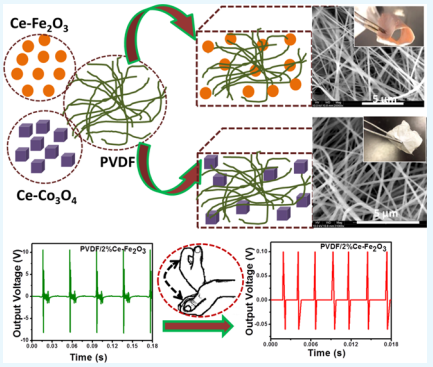


## 1. INTRODUCTION

Harvesting electrical energy from kinetic energy during various dynamic activities has attracted a wide research interest due to its renewable nature and easy availability.[1−3] Several studies have been conducted on electroactive polymers such as poly(vinylidene fluoride) (PVDF) and its copolymers like poly(vinylidene fluoride-trifluoroethylene) [P(VDF-TrFE)] and poly(vinylidene fluoride-hexafluoropropylene) [P(VDF-HFP)] in fabricating piezoelectric nanogenerators (PENG). These polymers possess outstanding piezoelectricity, ferroelectricity, and pyroelectricity.[4−6] They have various applications in transducers, sensors, and actuators because of their unique structural polymorphs.[7−9] In the semicrystalline PVDF, five polymorphs, $\alpha$, $\beta$, $\gamma$, $\delta$, and $\epsilon$, are present, among which the electroactive $\beta$ phase is the most polar and it is responsible for the high piezoelectric responses. To improve the piezoelectric performance of PVDF through $\beta$-phase nucleation, high field electric poling (70−80 MV/m) is often done. However, this external electric poling technique is cost-intensive, inconvenient, and not at all an industrial-friendly technique for large-scale manufacturing.[10,11]

One of the promising alternatives in this regard is the self-polarized PVDF-based PENG. Karan et al. developed PENGs based on self-polarized PVDF containing iron-doped reduced graphene oxide (Fe-RGO) nanosheets, without applying any electrical poling technique during fabrication.[12] They achieved high piezoelectric properties due to the presence of Fe-RGO nanofillers in the nanocomposite. The influence of ferrite nanoparticles in promoting electroactive $\beta$-phase nucleation is also reported in other studies.[13,14] Hoque et al.[15] fabricated PVDF films containing $Er^{3+}$ and $Fe^{3+}$ ions and investigated their piezoelectric properties in correlation with the electroactive $\beta$-phase nucleation and dielectric properties. They also reported the enhancement in the dielectric properties and crystallinity of PVDF by rare earth ion incorporation.[16] Cerium(III)/yttrium(III) nitrate hexahydrate in PVDF,[17] lanthanum(III) chloride in PVDF, $ErCl_3$ and $GdCl_3$ in PVDF, etc.[16] also substantiated enhanced dielectric properties and electroactive $\beta$-phase nucleation due to the less capability of covalent bond formation. Thus, the transition-metal cations influence the PVDF properties by affecting its chemical environment through covalent interactions.[18]

Even though there are several studies on the incorporation of rare earth ions in PVDF, most preparation methods have followed solution routes. A few reports also show PVDF nanofiber membranes with enhanced $\beta$-phase crystallinity using electrospinning technology. Such electrospun PVDF nanofibers report strong piezoelectricity omitting the need of

Received: January 27, 2019
Accepted: February 25, 2019
Published: April 4, 2019

  

DOI: 10.1021/acsomega.9b00243
ACS Omega 2019, 4, 6312−6323

further electrical poling treatments.[19−24] This is mainly because of the dipolar alignment induced by the presence of high voltage during spinning. The method of electrospinning has upraised as an effective method in producing self-poled piezoelectric nanofibers because of the high stretching forces exerted on electrified solution jets.[25]

Herein, we prepared PVDF nanofibers and its nanocomposites with Ce−$Fe_2O_3$ and Ce−$Co_3O_4$ at 2 wt % by electrospinning. The magnetic Ce−$Fe_2O_3$ and Ce−$Co_3O_4$ nanomaterials were synthesized by the hydrothermal method, in which the $Ce^{3+}$ ions control the metal oxide particle crystal size growth to great extents. The nanoparticles influenced the crystalline structure of PVDF, and the piezoelectric performance of the PENG is correlated with the composite's interfacial crystalline environment. The PENG based on Ce−$Fe_2O_3$ generated an output voltage of up to 20 V, which was reproducible and stable. Variation in output voltages of the PENGs was tested with human body movements, along with its durability. The surface electrostatic interactions existing within the polymer nanocomposite PENG and the electroactive $\beta$-phase nucleation of PVDF chains in the presence of the nanomaterials match well with the superior piezoelectric performance of the fabricated PENGs.

## 2. EXPERIMENTAL SECTION

**2.1. Materials.** PVDF pellets of $M_w \sim 275\,000$ g/mol, *N*,*N*-dimethylformamide (DMF), and acetone were purchased from Sigma-Aldrich. Other reagents such as monoethanolamine [$C_2H_7NO$] [MEA], poly(ethylene glycol) [PEG], iron(III) chloride 6-hydrate, cerium(III) chloride 7-hydrate, and cobalt(II) chloride 6-hydrate were also commercially obtained from Sigma-Aldrich.

**2.2. Synthesis of Pure and Ce-Doped Metal Oxide Nanoparticles.** Required amounts of iron(III) chloride 6-hydrate and cerium(III) chloride 7-hydrate (with molar ratio Fe/Ce = 1.94:0.06) were dissolved in 50 mL of distilled water, to which 0.5 g of PEG was added followed by 3 mL of MEA. The resulting solution was transferred to an autoclave at 120 °C temperature and kept for 2 h. The obtained precipitate was washed with water and ethanol several times to remove the soluble ions, dried at 80 °C for 3 h, followed by calcination in a tube furnace at 400 °C for 2 h. The obtained Ce−$Fe_2O_3$ was used for the analysis and for composite preparation. A similar process was done for the preparation of Ce−$Co_3O_4$ using cobalt(II) chloride 6-hydrate precursor.

**2.3. Fabrication of PVDF/Ce−$Fe_2O_3$ and PVDF/Ce−$Co_3O_4$ Nanocomposite Fibers.** PVDF pellets were dissolved in a 1:1 DMF/acetone solvent mixture to obtain a 17% polymer solution by magnetic stirring for 3 h at 70 °C. The magnetic Ce−$Fe_2O_3$ and Ce−$Co_3O_4$ nanoparticles at 2 wt % were separately dispersed in the same solvent mixture through bath sonication, then added to the PVDF dissolution, and further magnetically stirred overnight. These homogeneous dispersions of nanocomposites were used for electrospinning at 1 mL/h rate, as previously reported by our team.[26] The spun nanofibers were collected on a cylindrical rotor, rotating at 500 rpm, placed about 10 cm away from the needle tip at an applied voltage of 12 kV. The obtained nanofibers were silver-electroded on both sides, and a small PENG was designed by sandwiching between poly(dimethyl siloxane) (PDMS) sheets.

**2.4. Characterization of the Composite Nanofibers.** The structural properties of the nanopowders and the polymer composites were investigated using an X-ray diffractometer (MiniFlex 2, Rigaku, equipped with Nickel-filtered Cu K$\alpha$ radiation ($\lambda$ = 0.1564 nm) operated at 30 V and 15 mA in the $2\theta$ range of 10−30° at a scanning speed of 1.8°/min) and an Fourier transform infrared (FTIR) spectrometer (PerkinElmer Spectrum 400 spectrophotometer in the range of 400−4000 $cm^{-1}$ with a resolution of 2 $cm^{-1}$). The surface morphology was studied using a scanning electron microscope (SEM, XL-30E Philips Co., Holland) and a transmission electron microscope (TEM, FEI TECNAI $G^2$ TEM). The $\zeta$-potential measurements to determine the surface charge on the nanoparticles were performed by dispersing the nanoparticles in water using a Zetasizer Nano (Malvern) analyzer. X-ray photoelectron spectrum was recorded using Kratos Axis Ultra DLD. The dielectric properties were tested by broad-band dielectric/impedance spectroscopy (Novocontrol) in the frequency range of 10−$10^7$ Hz. The piezoelectric device fabrication and the testing system were similar to our previous reports.[2,26,27]

## 3. RESULTS AND DISCUSSION

**3.1. Structural Investigation and Morphology of Ce−$Fe_2O_3$ and Ce−$Co_3O_4$ Nanomaterials.** The X-ray diffraction (XRD) patterns of pure metal oxide ($Fe_2O_3$ and $Co_3O_4$) nanofillers and their cerium-doped counterparts reveal interesting crystalline structures (Supporting Information, Figure S1). The diffraction peaks found at 24.1, 33.19, 35.60, 40.88, 49.51, 54.00, 57.58, 62.37, 63.97, 71.87, and 75.47° correspond to the (012), (104), (110), (113), (024), (116), (018), (214), (300), (119), and (220) crystal planes, in the case of $Fe_2O_3$. These indexed diffraction peaks match well with the standard data for hematite $Fe_2O_3$ structure (powder diffraction file no. 98-016-4010 ICDD). Similarly, for the pure and Ce-doped $Co_3O_4$, the indexed diffraction peaks at 19.01, 31.34, 36.87, 38.53, 44.82, 55.67, 59.33, and 65.19° correspond to the (111), (220), (311), (222), (400), (422), (511), and (440) planes of $Co_3O_4$ cubic phase according to the powder diffraction card no. 98-002-4210 ICDD (Figure S1b). No other peaks corresponding to $Ce_2O_3$ and other impurities were detected, which confirms the phase purity of the samples. This also implies that the crystal structures of $Fe_2O_3$ and $Co_3O_4$ have not been altered due to the incorporation of $Ce^{3+}$ ions. In other words, the $Ce^{3+}$ ions are uniformly substituted into the Fe and Co lattice sites. Furthermore, the decrease in the peak intensity and broadening of the XRD peaks with incorporation of $Ce^{3+}$ ions (compared to the undoped metal oxides) implies smaller crystallite size for the Ce-doped $Fe_2O_3$ and $Co_3O_4$.

The crystallite size ($D$) is calculated by the following Scherrer equation

$$D = \frac{0.9\lambda}{\beta \cos\theta} \quad (1)$$

where $\lambda$ is the wavelength of the incident X-rays, $\theta$ is Bragg's angle of diffraction, and $\beta$ is the full width at half-maximum.[28] The calculated crystallite size was 45 nm for pure $Fe_2O_3$, whereas a smaller crystallite size of 39 nm was observed for the Ce-doped $Fe_2O_3$. Similarly, the crystallite sizes for $Co_3O_4$ and Ce-doped $Co_3O_4$ were 32 and 29 nm, respectively. For both Ce-doped metal oxides, the crystallite sizes were decreased, due to the lattice distortion and strain induced by the $Ce^{3+}$ ion substitutions, which in turn deteriorate the $Fe_2O_3$ and $Co_3O_4$ crystallinity.[29] The smaller crystallite size is an important



DOI: 10.1021/acsomega.9b00243
ACS Omega 2019, 4, 6312−6323

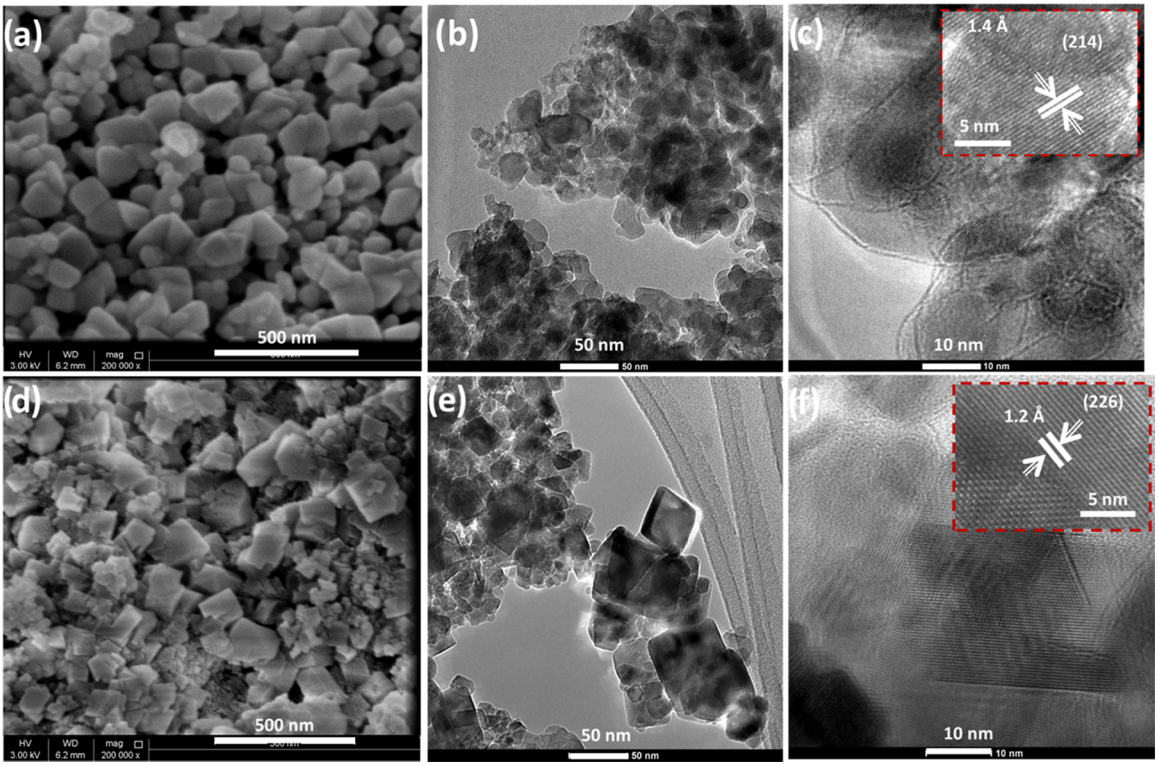


**Figure 1.** SEM and TEM images of (a–c) 3 wt % Ce-doped $Fe_2O_3$ and (d–f) 3 wt % Ce-doped $Co_3O_4$ samples.

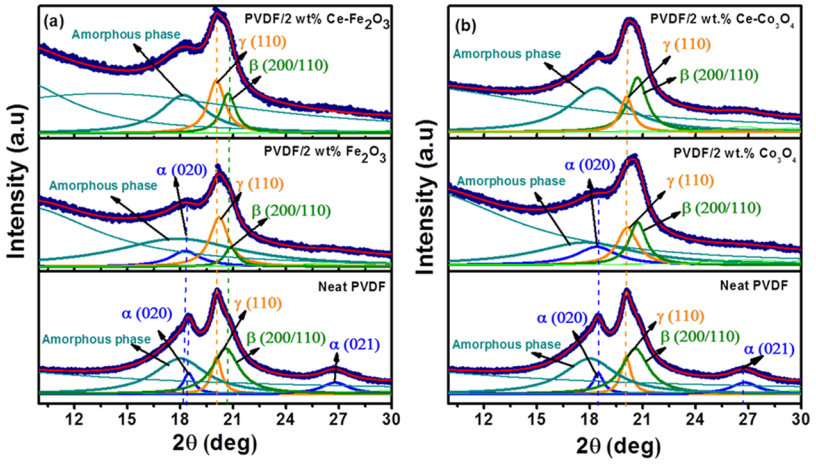


**Figure 2.** XRD patterns of (a) neat PVDF and PVDF/2 wt % $Fe_2O_3$ and PVDF/2 wt % Ce–$Fe_2O_3$ nanofibers and (b) neat PVDF and PVDF/2 wt % $Co_3O_4$ and PVDF/2 wt % Ce–$Co_3O_4$ nanofibers.

parameter for the enhancement in output power of the PENG designed out of it as well.[30]

The morphology of the synthesized nanomaterials is demonstrated in Figure 1. The SEM and TEM images in Figure 1a–c for the 3 wt % Ce-doped $Fe_2O_3$ show spherical morphology and uniform distribution with less agglomeration. From the SEM and TEM images of 3 wt % Ce-doped $Co_3O_4$ samples (Figure 1d–f), the cubic morphology is identified. These results suggest that the $Fe_2O_3$ and $Co_3O_4$ lattices were not much disturbed by the incorporation of $Ce^{3+}$ ions. The high-resolution TEM images of the 3 wt % Ce-doped $Fe_2O_3$ and 3 wt % Ce-doped $Co_3O_4$ samples reveal fringe spacings of 1.4 and 1.2 Å, respectively, corresponding to the (214) and (226) crystal planes of $Fe_2O_3$ and $Co_3O_4$ nanomaterials.

**3.2. Structural Properties and Morphology of PVDF/Ce–$Fe_2O_3$ and PVDF/Ce–$Co_3O_4$ Nanofibers.** Figure 2 shows the XRD patterns of neat PVDF and its nanocomposites containing $Fe_2O_3$, Ce–$Fe_2O_3$, $Co_3O_4$, and Ce–$Co_3O_4$ nanomaterials. The electroactive $\beta$- and $\gamma$-phases are evaluated from the deconvoluted XRD plots, as indicated in Figure 2. The indexed diffraction peaks at $2\theta$ values of 18.3 and 26.8° correspond to the (020) and (021) planes of $\alpha$-crystalline phase.[31,32] The diffraction peaks at 20.6° (200/110) and 20.1° (110) are attributed to the presence of $\beta$-phase with the coexistence of the $\gamma$ phase.[33,34] The two $\alpha$-characteristic peaks for neat PVDF were diminished with the addition of nano-Ce–$Fe_2O_3$ and Ce–$Co_3O_4$ into the PVDF matrix and only the electroactive $\gamma$ and $\beta$ phases were observed. The improved electroactive phase formation is clear from the XRD peaks of



DOI: 10.1021/acsomega.9b00243
ACS Omega 2019, 4, 6312–6323

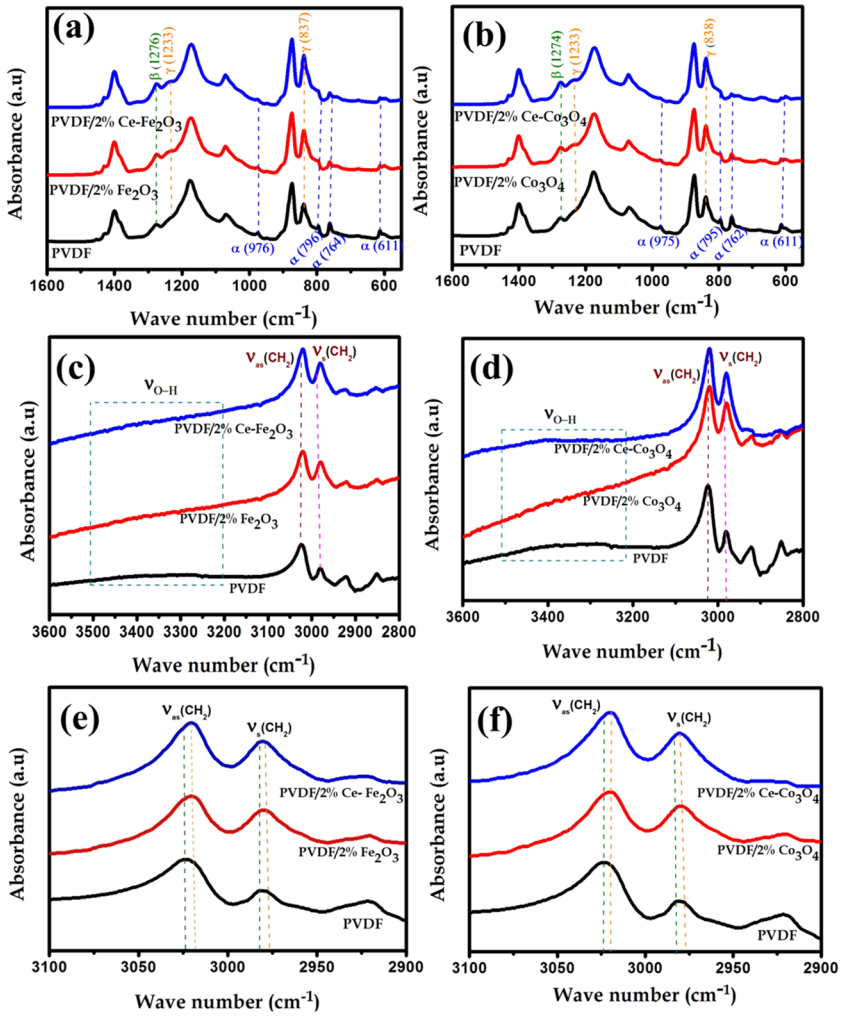


**Figure 3.** FTIR patterns of neat PVDF and PVDF/Ce−$Fe_2O_3$ and PVDF/Ce−$Co_3O_4$ nanofibers in the regions 1600−500 $cm^{-1}$ (a, b), 3600−2800 $cm^{-1}$ (c, d), and 3100−2900 $cm^{-1}$ (e, f).

the Ce-doped metal oxides containing PVDF. These electroactive phases are responsible for the enhancement in the piezoelectric properties of PVDF-based PENGs.

FTIR spectroscopy is a powerful tool to study the crystalline phase formation in PVDF nanocomposites. Figure 3 shows the FTIR spectra of neat PVDF and PVDF/2 wt % Ce−$Fe_2O_3$ and PVDF/2 wt % Ce−$Co_3O_4$ nanofibers. The absorption bands observed at 976, 796, 764, and 611 $cm^{-1}$ correspond to the nonpolar $\alpha$-phase of PVDF, whereas the characteristic peaks at 1276, 1233, and 837 $cm^{-1}$ correspond to the electroactive $\beta$ and $\gamma$-phases.[35−37] All of the characteristic absorption bands due to the $\alpha$-phase diminish in the case of PVDF composite nanofibers, compared to the neat polymer, and only the characteristic absorption bands due to electroactive $\beta$ and $\gamma$-phases exist. In addition, the intensities of both $\beta$ and $\gamma$-phases of PVDF characteristic bands were increased for the Ce−$Fe_2O_3$ and Ce−$Co_3O_4$ filled fibers compared to the neat PVDF.

This is due to the interfacial interaction between the nanofillers (both Ce−$Fe_2O_3$ and Ce−$Co_3O_4$) and −$CH_2$−/−$CF_2$− dipoles of the PVDF chain, which leads to the formation of electroactive phases.[38] These interfacial interactions are also demonstrated by X-ray photoelectron spectroscopy (XPS) and $\zeta$-potential studies, described in the following sections of this study. Figure 3c,d shows FTIR spectra in the 3600−2800 $cm^{-1}$ region, indicating the formation of intermolecular H-bonds between PVDF and the magnetic nanomaterials.[39] The two fundamental vibrational bands for −$CH_2$− asymmetric ($\nu_{as}$) and symmetric ($\nu_s$) stretching vibrations were shifted to lower-frequency region, due to the same interfacial interaction caused by the positively charged surface of the Ce-doped $Fe_2O_3$ and $Co_3O_4$ nanofillers and −$CF_2$− dipoles of the PVDF matrix.[40]

The relative fraction of the electroactive $\gamma$-phase content ($F(\gamma)$) in the PVDF/Ce−$Fe_2O_3$ and PVDF/Ce−$Co_3O_4$ nanofibers is calculated by using the following equation[34]

$$F(\gamma) = \frac{X(\gamma)}{X(\alpha) + X(\gamma)} = \frac{A(\gamma)}{(K(\gamma)/K(\alpha))A(\alpha) + A(\gamma)} \quad (2)$$

where $A_\alpha$ and $A_\gamma$ are the areas of absorption peaks for the $\alpha$ and $\gamma$ phases (at 764 and 837 $cm^{-1}$), respectively; $X_\alpha$ and $X_\gamma$, respectively, represent the crystallinities of the $\alpha$ and $\gamma$ phases; and $K_\alpha$ and $K_\gamma$ are the absorption coefficients with values of 0.365 and 0.150 $\mu m^{-1}$, respectively. According to the equation, the $\gamma$-phase contents in the PVDF and its nanocomposites were estimated as shown in Table S1. The relative electroactive $\gamma$-phase fraction was found to be higher for the PVDF nanocomposites than for the neat PVDF. These results can be attributed to the smaller crystallite sizes of Ce−$Fe_2O_3$ and Ce−$Co_3O_4$ nanoparticles. Liu et al.[41] also suggested similar



DOI: 10.1021/acsomega.9b00243
ACS Omega 2019, 4, 6312−6323

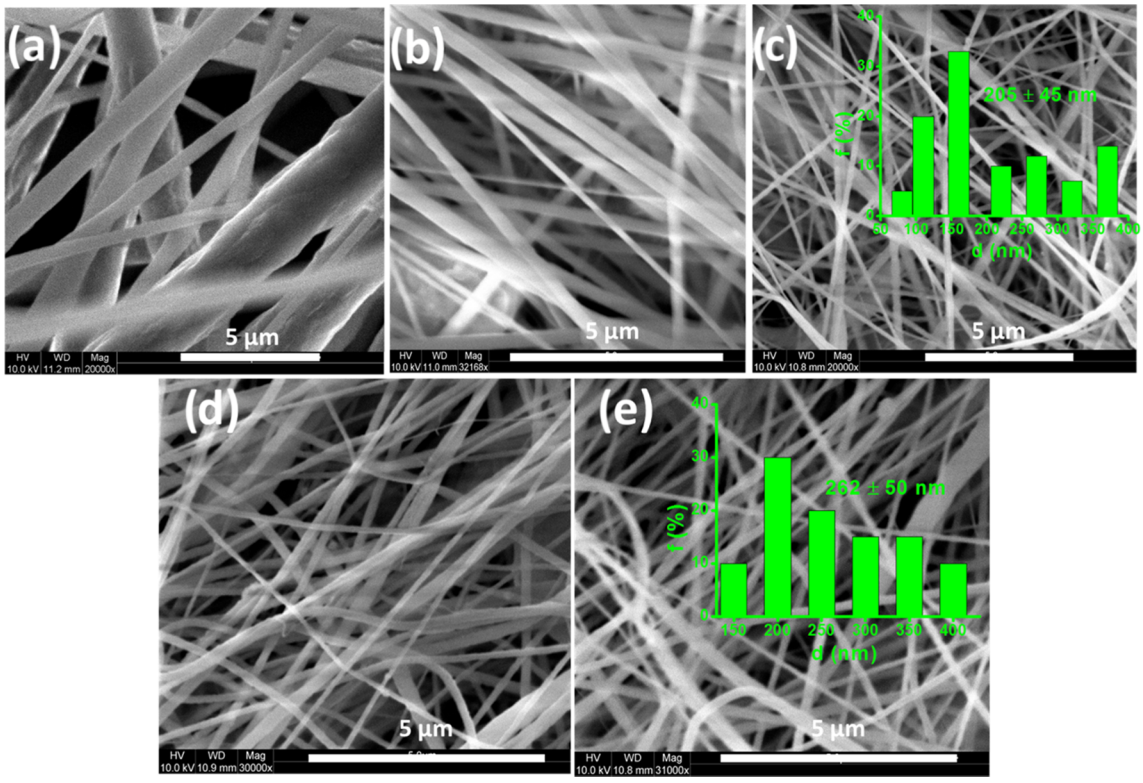


**Figure 4.** SEM images of neat PVDF (a), PVDF/2 wt % $Fe_2O_3$ (b), PVDF/2 wt % Ce−$Fe_2O_3$ (c), PVDF/2 wt % $Co_3O_4$ (d), and PVDF/2 wt % Ce−$Co_3O_4$ (e) samples. The inset shows the distribution of fiber diameter for the composite nanofibers containing Ce-doped metal oxides.

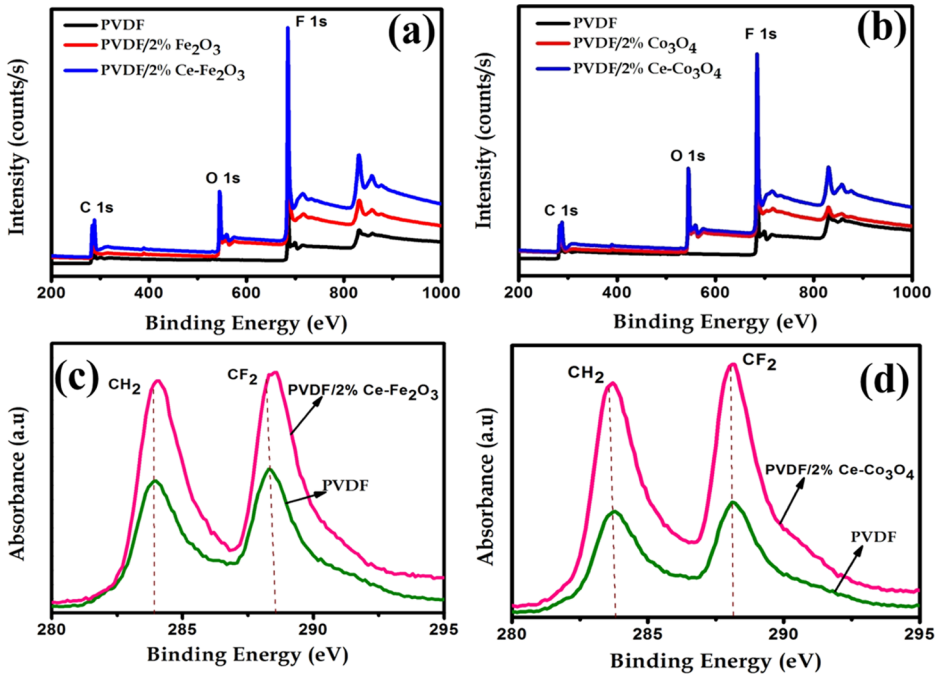


**Figure 5.** (a, b) Survey spectra of neat PVDF and PVDF/2 wt % Ce−$Fe_2O_3$ and PVDF/2 wt % Ce−$Co_3O_4$ nanofibers and (c, d) C 1s spectrum of neat PVDF and PVDF/2 wt % Ce−$Fe_2O_3$ and PVDF/2 wt % Ce−$Co_3O_4$ nanofibers.

stabilization of γ-phase due to the positive charges present in the nanoparticles that interact with the $-CF_2-$ dipoles of the PVDF chains.

The SEM images of neat PVDF and its composite nanofibers are shown in Figure 4. The nanofibers are smoother and defect-free as observed. In the PVDF composite nanofibers, the nanoparticles are well dispersed within the polymer as beads are not observed on the surfaces, which is due to an increased charge density of the polymer solution.[42] In addition, no surface defects/cracks are observed on the surface of the composite nanofibers. These results suggest the flexibility of the nanocomposite fibers, and moreover the



DOI: 10.1021/acsomega.9b00243
ACS Omega 2019, 4, 6312−6323

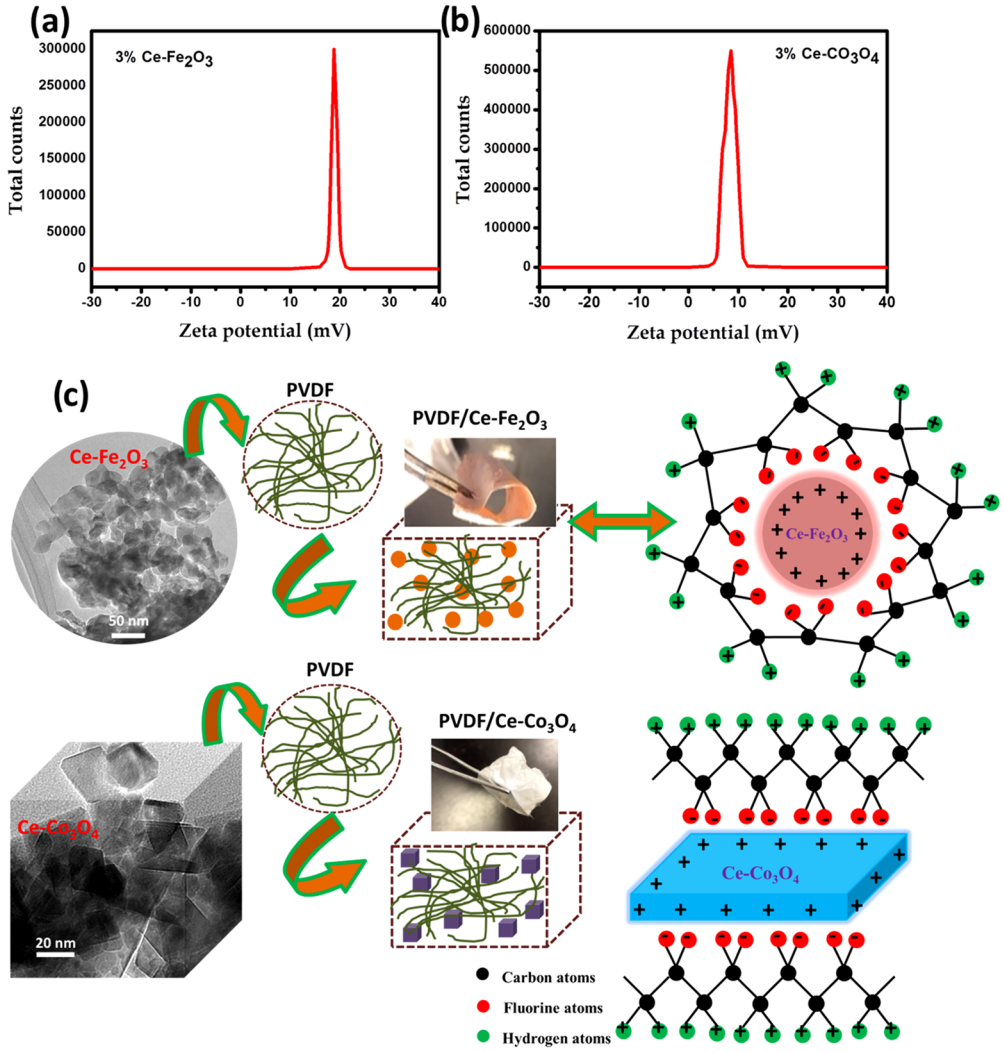


**Figure 6.** (a, b) ζ-Potential distribution of 3 wt % Ce−$Fe_2O_3$ and 3 wt % Ce−$Co_3O_4$ nanoparticles. (c) Schematic representation of the interaction between positively charged nanoparticles and PVDF molecules.

magnetic Ce−$Fe_2O_3$ and Ce−$Co_3O_4$ nanomaterials did not make the polymer brittle.[43] Further investigation on the average fiber diameter for both PVDF/Ce−$Fe_2O_3$ (205 ± 45 nm) and PVDF/Ce−$Co_3O_4$ (262 ± 50 nm) nanofibers reveals a higher value for the latter. The morphology of the nanofibers was further investigated by TEM (Supporting Information, Figure S2). The TEM images of PVDF nanofibers containing Ce−$Fe_2O_3$ and Ce−$Co_3O_4$ nanoparticles demonstrate the uniform filler distribution in PVDF without any aggregation.

The filler−polymer interfacial interactions were further investigated by XPS.[44,45] Figure 5 shows the XPS images of neat PVDF and PVDF/2 wt % Ce−$Fe_2O_3$ and PVDF/2 wt % Ce−$Co_3O_4$ nanofibers. The strong peaks appearing at 282−288 and 688 eV correspond to the fluorine and carbon atoms in the PVDF skeleton. The C 1s spectrum of PVDF and its composite nanofibers are shown in Figure 5c,d. The strong peaks at 282 and 283 eV correspond to the $-CH_2$ and $-CF_2$ groups of PVDF.[46,47] In the XPS images, the peak intensity was increased and shifted for composite nanofibers, which suggests higher interfacial interaction existing between the PVDF dipoles and Ce-doped $Fe_2O_3$ and Ce-doped $Co_3O_4$ nanomaterials. Moreover, the increased peak intensity in the XPS images is ascribed to the existence of magnetic nanoparticles, which is in good agreement with the XRD and FTIR results for interfacial interactions.

**3.3. Electroactive β and γ-Phase Formation Mechanism in PVDF/Ce−$Fe_2O_3$ and PVDF/Ce−$Co_2O_3$ Nanofibers.** The formation of electroactive β and γ-phases has been confirmed by the XRD and FTIR results, by which an increase in electroactive phase nucleation was noted with the introduction of magnetic nanoparticles. It is necessary to study the interaction between the magnetic nanoparticles and PVDF matrix since it promotes the formation of the electroactive phase. The transformation of α-phase to the electroactive β-phase in PVDF may be due to the electrostatic interaction between the PVDF matrix and the magnetic nanoparticles.[48] Karan et al. suggested that the addition of positively charged iron-doped reduced graphene oxide interacts with the $-CF_2-$ dipoles of PVDF matrix and causes the crystallization transformation from α-phase to γ-phase.[12] He et al. also addressed the formation of electroactive phases by the electrical interfacial interaction between the positively charged organosilicate surface and the partially negative $-CF_2-$ bonds of the PVDF matrix.[49]

To address the surface electrostatic interactions between the cerium-doped metal oxides and the PVDF chains, ζ-potential studies are rather necessary. The surface electrostatic charges



DOI: 10.1021/acsomega.9b00243
ACS Omega 2019, 4, 6312−6323

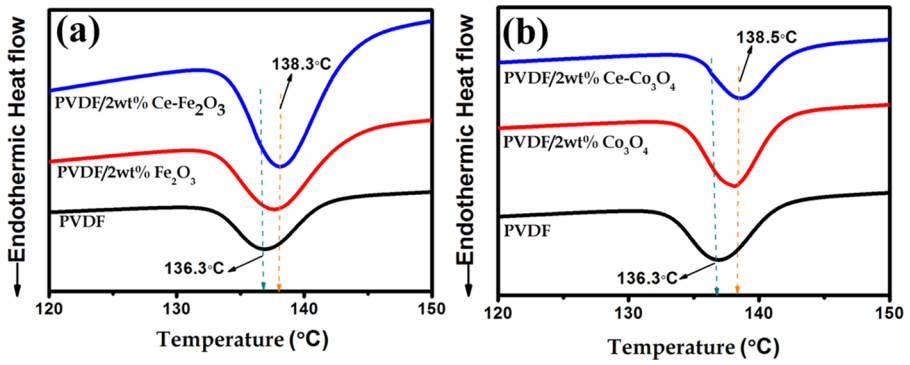


**Figure 7.** (a, b) DSC thermograms of PVDF, PVDF/2 wt % Ce−$Fe_2O_3$, and PVDF/2 wt % Ce−$Co_3O_4$.

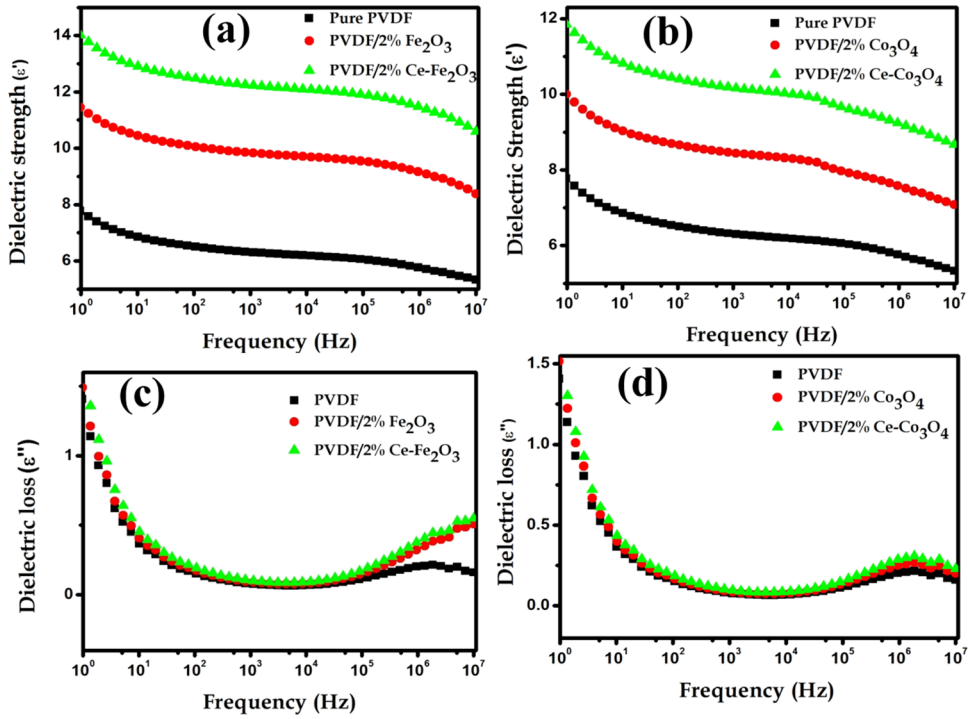


**Figure 8.** Variation of dielectric constant (a, b) and dielectric loss (c, d) of the PVDF and PVDF/2 wt % Ce−$Fe_2O_3$ and PVDF/2 wt % Ce−$Co_3O_4$ nanofibers with frequency.

of the Ce-doped $Fe_2O_3$ and Ce-doped $Co_3O_4$ nanoparticles obtained from the $\zeta$-potential analysis are demonstrated in Figure 6a,b. From these results, the surfaces of the magnetic nanoparticles were identified to be positively charged, which interact with the $-CF_2-$ dipoles of PVDF via local ion−dipole electrostatic interactions. These electrostatic interactions lead to the formation of electroactive phases within the polymer units. Thus, the surface of each nanoparticle acts as a nucleation center for the formation of electroactive phases. The proposed interfacial interaction mechanism between the magnetic nanoparticles and the PVDF matrix is schematically represented in Figure 6c. A similar effect of interaction with the positively charged nanoparticles and the $-CF_2-$ dipoles of the PVDF chains, through which the stabilization of $\gamma$-phase was achieved was reported by Liu et al.[41] Moreover, Liang et al. suggested the formation of electroactive phases in PVDF due to the ion−dipole interactions between the positively charged molecules and $-CF_2-$ dipoles in PVDF or the negatively charged molecules and the $-CH_2-$ dipoles in PVDF chains.[50]

**3.4. Crystallization Behavior of PVDF/Ce−$Fe_2O_3$ and PVDF/Ce−$Co_2O_3$ Nanofibers.** Figure 7 displays the differential scanning calorimetry (DSC) curves of neat PVDF, PVDF/2 wt % Ce−$Fe_2O_3$, and PVDF/2 wt % Ce−$Co_3O_4$ samples. Here, the observed exothermic peak corresponds to the crystallization temperature of neat PVDF and its composite nanofibers. Compared to the neat PVDF, the crystallization temperature was higher for the composite fibers. These results further confirm the nucleating action of nanofillers and their role in accelerating the PVDF crystallization.[51]

The degree of crystallinity was calculated by using the following equation

$$X_C = \frac{\Delta H_m}{\Delta H_{mo}} \times 100 \quad (3)$$

where $\Delta H_m$ is the melting enthalpy of the nanocomposites and $\Delta H_{mo}$ is the melting enthalpy of the 100% crystalline PVDF (104.5 J/g).[52] The degree of crystallinity values thus calculated are tabulated in Table S1 (Supporting Information). It is found that the composite nanofibers containing Ce−$Fe_2O_3$ and Ce−



DOI: 10.1021/acsomega.9b00243
ACS Omega 2019, 4, 6312−6323

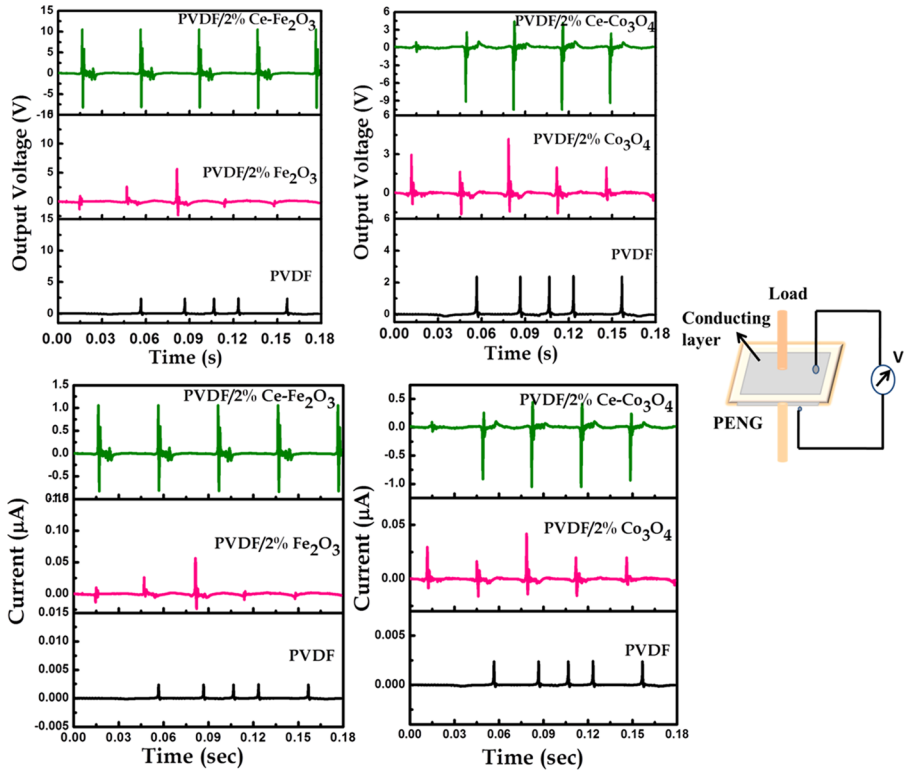


**Figure 9.** (a–d) Output voltages and output currents from the piezoelectric nanogenerator fabricated with neat PVDF and PVDF/2 wt % Ce–$Fe_2O_3$ and PVDF/2 wt % Ce–$Co_3O_4$ nanofibers.

$Co_3O_4$, respectively, show crystallinity values of 43.6 and 43.2% compared to the neat PVDF fiber (41.2%). This higher percentage of crystallinity achieved for the nanocomposite suggests the electroactive $\beta$-phase formation[26] further and is in good correlation with the XRD and FTIR analyses.

**3.5. Dielectric Properties of PVDF/Ce–$Fe_2O_3$ and PVDF/Ce–$Co_2O_3$ Nanofibers.** Figure 8 shows the frequency-dependent dielectric properties of neat PVDF and PVDF/2 wt % Ce–$Fe_2O_3$ and PVDF/2 wt % Ce–$Co_3O_4$ nanofibers. Both dielectric constant and loss values increase in the low-frequency region and decrease in the high-frequency region. The increase in dielectric constant and its reduction with increasing frequency is attributed to the high interfacial polarization originated from the Maxwell–Wagner–Sillars polarization effect, which causes the accumulation of charge carriers at the PVDF/nanoparticles interface.[53−55] Paria et al. also suggested a similar increase in dielectric constant due to the decrease in filler–filler distances and higher dipole–dipole polarization in the nanocomposites.[56]

The observed dielectric constants for the PVDF composites of Ce-doped $Fe_2O_3$ and Ce-doped $Co_3O_4$ were higher than that of neat PVDF, and the values were, respectively, 14 and 12. This is because of the large accumulation of charge carriers at the interface between magnetic nanoparticles and PVDF. Thakur et al. illustrated that the small crystallite size with large surface area of nanoparticles leads to good homogeneous dispersion in the polymer and creates large interfacial areas between the nanoparticles and PVDF matrix. This causes large accumulation of the charge carriers and enhanced dielectric constant.[57] The conductivity values of the composites (Supporting Information, Figure S3) increased with increasing frequency, and the values were in the order of $10^{-14}$ S/cm in the lower-frequency region for all PVDF fibers studied. This also suggests the Maxwell–Wagner–Sillars effect existing in the interface of PVDF/nanoparticles.[18]

**3.6. Piezoelectric Properties of PVDF/Ce–$Fe_2O_3$ and PVDF/Ce–$Co_2O_3$ Nanofibers.** Both PVDF/Ce–$Fe_2O_3$ and PVDF/Ce–$Co_3O_4$ electrospun fiber mats were cut into smaller circular pieces of 2 cm diameter and electroded on both sides using aluminum foil and silver paste. Separate wires were also attached on both sides and the piezoelectric output performances were recorded with the help of an already established setup.[26,27] This assembled setup contains a vibrating shaker, on top of which the sample will be placed with a force of 2.5 N. Depending on the input values in frequency generator, the shaker vibrates, causing a compressive force on the sample by means of the force applied on it. These mechanical vibrations were transformed to electrical potential differences, which is obtained by a data acquisition system. Both sides of the samples were connected directly to a resistor box, the variations of which can optimize the best output current and voltage and thus the power. The generated output voltage from the PVDF-based fiber PENG as a function of time is shown in Figure 9a,b. The schematic representation of the PENG is also shown in the same figure. The highest output peak-to-peak voltages of 20 and 15 V were, respectively, observed for the PVDF/Ce–$Fe_2O_3$ and PVDF/Ce–$Co_3O_4$ nanofibers, much higher than the neat PVDF. All of the composite nanofibers showed excellent output performance without requiring any external electric poling and direct contact with the device.[19] The enhanced output voltages for the nanofibers containing Ce-doped metal oxides may be due to the induced electroactive phases within the composite and the electrostatic interactions between the nanomaterials and the PVDF. This interaction played a significant role in inducing self-polarization within the composites.[58] The interaction between the



DOI: 10.1021/acsomega.9b00243
ACS Omega 2019, 4, 6312−6323

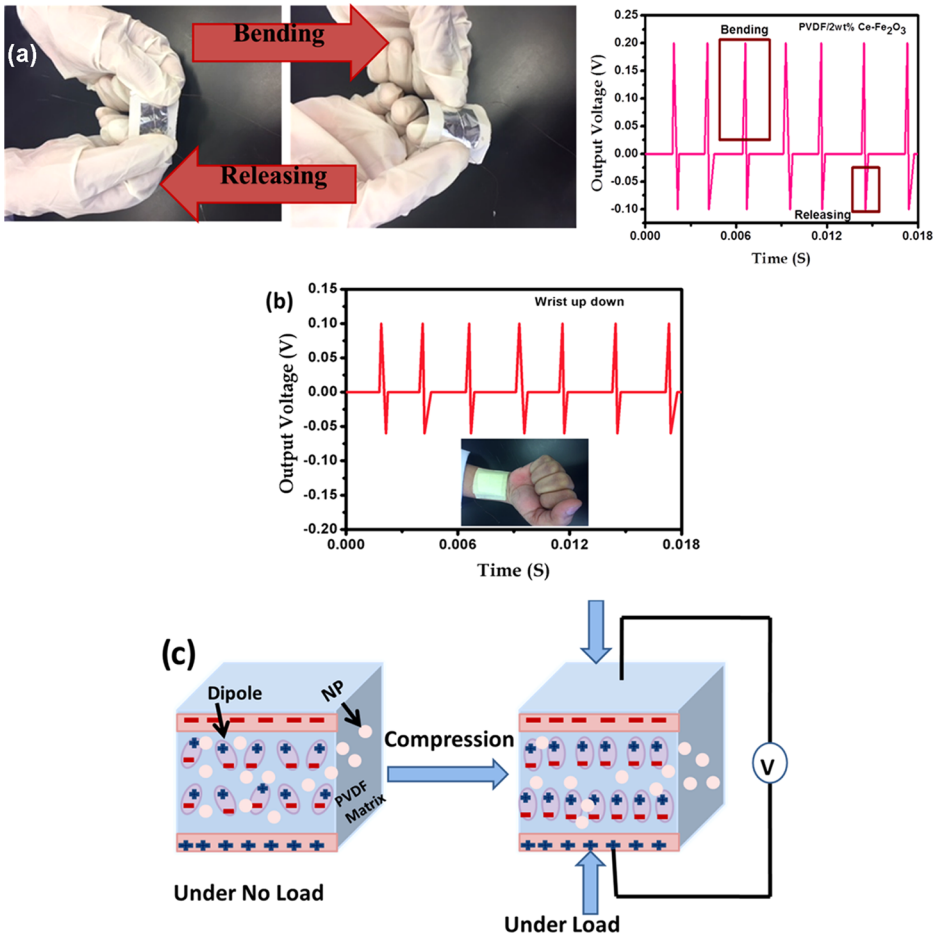


**Figure 10.** (a) Bending and releasing movements of the PENG based on PVDF/Ce−$Fe_2O_3$. (b) Output performance when subjected to wrist movements. (c) Schematic illustration of the piezoelectric effect.

nanoparticles and the PVDF chains improved the polarization ordering and increased the stability of the molecular chain that lead to a better degree of alignment of the dipoles. Finally, the dipoles of the PVDF molecules were self-polarized along specific directions due to the effect of stress- and surface charge-induced polarization. Mandal et al. also made a similar observation that the improvement in output voltage comes from the large content of electroactive $\beta$-phase and self-poling induced by the presence of Ag nanoparticles in PVDF-HFP.[42] Moreover, the crystal deformation in the nanocomposites has a significant effect on the output performance of the flexible PENG.[59,39] These variable dipoles within the nanocomposite depends on the nature of filler material and the charge−discharge processes taking place upon mechanical deformation. And this is the reason for the small variations in the output voltage characteristics observed in the case of PVDF nanocomposites.

The piezoelectric output current performance is shown in Figure 9c,d. The maximum output currents for the PVDF/Ce−$Fe_2O_3$ and PVDF/Ce−$Co_3O_4$ nanofibers were 2.2 and 1.44 $\mu$A, respectively. The piezoelectric output power can be calculated by using the following relation.

$$\text{power density} = \frac{\text{voltage} \times \text{current}}{\text{area} \times \text{thickness}} \quad (4)$$

The power density values obtained for the PVDF/Ce−$Fe_2O_3$ and PVDF/Ce−$Co_3O_4$ composite fibers were 700.64 and 334.39 $\mu A/cm^3$, respectively. As reported earlier in the structure and morphology of the nanocomposites, the enhanced output performance of the PENG is due to the better dispersion of nanoparticles in the PVDF.[60] In other words, the enhanced piezoelectric output can be attributed to the combinational effect of the oriented electroactive phase and the surface electrostatic interaction between the nanoparticles and the PVDF matrix. It is also noteworthy that the Ce−$Fe_2O_3$ composite possesses comparatively higher performance than Ce−$Co_3O_4$, which again can be correlated with the morphology and surface interactions. The spherical uniform structure of Ce−$Fe_2O_3$ allows maximum surface area to interact with the PVDF chains, whereas the cubic structures sometimes hinder the polymer chains from good electrostatic interactions. Moreover, the particle sizes were also found to be lower for Ce−$Fe_2O_3$. Finally, the resultant output voltage and output current for the PVDF/Ce−$Fe_2O_3$ and PVDF/Ce−$Co_3O_4$ nanofibers reveal the application of PENGs in many low-powered portable electronic devices.

The stability of the piezoelectric output performance is also investigated by monitoring the output voltage for a few hours.[61] This is represented in Figure S4 (Supporting Information), from which the long-term stability (over 2 h) for the two systems, PVDF/Ce−$Fe_2O_3$ and PVDF/Ce−$Co_3O_4$ nanofibers, is evidenced.

To check the real-time applications of the fabricated PENGs, the one containing Ce−$Fe_2O_3$ (with comparatively high



DOI: 10.1021/acsomega.9b00243
ACS Omega 2019, 4, 6312−6323

power) was tested for the bending movements. Figure 10a shows the bending and releasing movements of the flexible PENG and its output performance. The observed positive and negative piezo-voltage peaks correspond to the bending and releasing vibrations. Later, the PENG is attached to the human wrist and the piezoelectric responses based on wrist movements are recorded (Figure 10b). In both bending and human wrist movements, the output voltage shows a notable variation indicating the application of the PENG in fabricating self-powering devices.

A schematic diagram for the piezoelectric mechanism occurring in a PVDF nanocomposite is shown in Figure 10c. When there is no applied force onto the sample, the net dipoles within the nanocomposites cancel each other, resulting in lower potential across the material. However, when a mechanical force is applied to the PVDF nanofiber, a potential is created in the magnetic nanoparticles and helps the PVDF dipoles to align through stress-induced polarization. This self-polarization is responsible for the high piezoelectric output performance. Most of the polymer nanocomposites show piezoelectricity because of such self-polarization induced by the nanoparticles. And in addition, this self-polarization depends on the nature and type of nanomaterials, their alignment, and the surface electrostatic interfacial interactions between the polymer and the nanomaterials.

## 4. CONCLUSIONS

We have successfully prepared new PVDF composite nanofibers using the electrospinning technique. Both the Ce-doped $Fe_2O_3$ and Ce-doped $Co_3O_4$ magnetic nanoparticles-loaded PVDF nanofibers showed enhanced $\beta$-phase crystallinity and piezoelectric property compared to the neat PVDF due to smaller crystallite size distribution and higher electrostatic interfacial interaction. The self-polarization, small crystallite size, and high $\beta$-phase crystallinity of PVDF upon nanoparticles loading have a significant influence on the enhanced piezoelectric property of PVDF/Ce−$Fe_2O_3$ and PVDF/Ce−$Co_3O_4$ nanofibers. The application of PENGs based on these nanocomposites is demonstrated by the bending and human wrist movements. In both movements, the output voltage was generated, confirming the successful use of the obtained PVDF nanocomposite in flexible self-powering devices.

## ■ ASSOCIATED CONTENT

### Supporting Information

The Supporting Information is available free of charge on the ACS Publications website at DOI: 10.1021/acsomega.9b00243.

Structural analysis of the Ce-doped $Fe_2O_3$ and Ce-doped $Co_3O_4$ nanomaterials via XRD studies (Figure S1); electrospun fiber morphology for the PVDF/Ce−$Fe_2O_3$ and PVDF/Ce−$Co_3O_4$ nanocomposites (Figure S2); conductivity spectra of the composites (Figure S3); stability of output voltage for the PVDF/Ce-doped $Fe_2O_3$ and PVDF/Ce-doped $Co_3O_4$ nanofibers over time (Figure S4); and $\beta$-phase crystallinity values (Table S1) (PDF)

## ■ AUTHOR INFORMATION


### Corresponding Author

*E-mail: lekshmi_deepa@yahoo.com. Tel: +974 (4403) 5684.

### ORCID

Deepalekshmi Ponnamma: 0000-0002-5208-4870


### Notes

The authors declare no competing financial interest.

## ■ ACKNOWLEDGMENTS

This publication was made possible by NPRP grant 6-282-2-119 from the Qatar National Research Fund (a member of Qatar Foundation). The statements made herein are solely the responsibility of the authors.

## ■ REFERENCES


(1) Wang, X.; Song, J.; Liu, J.; Wang, Z. L. Direct-current nanogenerator driven by ultrasonic waves. *Science* **2007**, *316*, 102−105.

(2) Ponnamma, D.; Erturk, A.; Parangusan, H.; Deshmukh, K.; Ahamed, M. B.; Al-Maadeed, M. A. Stretchable quaternary phasic PVDF-HFP nanocomposite films containing graphene-titania-SrTiO3 for mechanical energy harvesting. *Emerg. Mater.* **2018**, *1*, 55−65.

(3) Persano, L.; Dagdeviren, C.; Su, Y.; Zhang, Y.; Girardo, S.; Pisignano, D.; Huang, Y.; Rogers, J. A. High performance piezoelectric devices based on aligned arrays of nanofibers of poly(vinylidenefluoride-co-trifluoroethylene). *Nat. Commun.* **2013**, *4*, No. 1633.

(4) Al-Saygh, A.; Ponnamma, D.; AlMaadeed, M. A.; Vijayan, P. P.; Karim, A.; Hassan, M. K. Flexible pressure sensor based on PVDF nanocomposites containing reduced graphene oxide-titania hybrid nanolayers. *Polymers* **2017**, *9*, 33.

(5) Martins, P.; Silva, M.; Lanceros-Mendez, S. Determination of the magnetostrictive response of nanoparticles via magnetoelectric measurements. *Nanoscale* **2015**, *7*, 9457−9461.

(6) Fang, H.; Li, Q.; He, W.; Li, J.; Xue, Q.; Xu, C.; Zhang, L.; Ren, T.; Dong, G.; Chan, H. L.; Dai, J.; Yan, Q. A high performance triboelectric nanogenerator for self-powered non-volatile ferroelectric transistor memory. *Nanoscale* **2015**, *7*, 17306−17311.

(7) Satapathy, K. D.; Deshmukh, K.; Ahamed, M. B.; Sadasivuni, K. K.; Ponnamma, D.; Pasha, S. K.; AlMaadeed, M. A.; Ahmad, J. High-quality factor poly (vinylidenefluoride) based novel nanocomposites filled with graphene nanoplatelets and vanadium pentoxide for high-Q capacitor applications. *Adv. Mater. Lett.* **2017**, *8*, 288−294.

(8) Chamakh, M. M.; Ponnamma, D.; Al-Maadeed, M. A. Vapor sensing performances of PVDF nanocomposites containing titanium dioxide nanotubes decorated multi-walled carbon nanotubes. *J. Mater. Sci.: Mater. Electron.* **2018**, *29*, 4402−4412.

(9) Ponnamma, D.; Goutham, S.; Sadasivuni, K. K.; Rao, K. V.; Cabibihan, J. J.; Al-Maadeed, M. A. Controlling the sensing performance of rGO filled PVDF nanocomposite with the addition of secondary nanofillers. *Synth. Met.* **2018**, *243*, 34−43.

(10) Ramadan, K. S.; Sameoto, D.; Evoy, S. A review of piezoelectric polymers as functional materials for electromechanical transducers. *Smart Mater. Struct.* **2014**, *23*, No. 033001.

(11) Chinya, I.; Pal, A.; Sen, S. Polyglycolated zinc ferrite incorporated poly (vinylidene fluoride)(PVDF) composites with enhanced piezoelectric response. *J. Alloys Compd.* **2017**, *722*, 829−838.

(12) Karan, S. K.; Mandal, D.; Khatua, B. B. Self-powered flexible Fe-doped RGO/PVDF nanocomposite: an excellent material for a piezoelectric energy harvester. *Nanoscale* **2015**, *7*, 10655−10666.

(13) Martins, P.; Costa, C. M.; Benelmekki, M.; Botelho, G.; Lanceros-Mendez, S. On the origin of the electroactive poly (vinylidene fluoride) $\beta$-phase nucleation by ferrite nanoparticles via surface electrostatic interactions. *CrystEngComm* **2012**, *14*, 2807−2811.

(14) Ouyang, Z. W.; Chen, E. C.; Wu, T. M. Enhanced piezoelectric and mechanical properties of electroactive polyvinylidene fluoride/iron oxide composites. *Mater. Chem. Phys.* **2015**, *149−150*, 172−178.




DOI: 10.1021/acsomega.9b00243
*ACS Omega* 2019, 4, 6312−6323

(15) Hoque, N. A.; Thakur, P.; Roy, S.; Kool, A.; Bagchi, B.; Biswas, P.; Saikh, M. M.; Khatun, F.; Das, S.; Ray, P. P. Er3+/Fe3+ Stimulated electroactive, visible light emitting, and high dielectric flexible PVDF film based piezoelectric nanogenerators: A simple and superior self-powered energy harvester with remarkable power density. *ACS Appl. Mater. Interfaces* **2017**, *9*, 23048−23059.
(16) El-Sayed, S. Optical properties and dielectric relaxation of polyvinylidene fluoride thin films doped with gadolinium chloride. *Phys. B* **2014**, *454*, 197−203.
(17) Thakur, P.; Kool, A.; Bagchi, B.; Hoque, N. A.; Das, S.; Nandy, P. The role of cerium (iii)/yttrium (iii) nitrate hexahydrate salts on electroactive $\beta$ phase nucleation and dielectric properties of poly (vinylidene fluoride) thin films. *RSC Adv.* **2015**, *5*, 28487−28496.
(18) Parangusan, H.; Ponnamma, D.; AlMaadeed, M. A. Investigation on the effect of $\gamma$-irradiation on the dielectric and piezoelectric properties of stretchable PVDF/Fe−ZnO nanocomposites for self-powering devices. *Soft Matter* **2018**, *14*, 8803−8813.
(19) Li, B.; Zhang, F.; Guan, S.; Zheng, J.; Xu, C. Wearable piezoelectric device assembled by one-step continuous electrospinning. *J. Mater. Chem. C* **2016**, *4*, 6988−6995.
(20) Fang, J.; Wang, X.; Lin, T. Electrical power generator from randomly oriented electrospun poly (vinylidene fluoride) nanofibre membranes. *J. Mater. Chem.* **2011**, *21*, 11088−11091.
(21) Mandal, D.; Yoon, S.; Kim, K. J. Origin of piezoelectricity in an electrospun poly (vinylidene fluoride-trifluoroethylene) nanofiber web-based nanogenerator and nano-pressure sensor. *Macromol. Rapid Commun.* **2011**, *32*, 831−837.
(22) Li, B.; Xu, C.; Zheng, J.; Xu, C. Sensitivity of pressure sensors enhanced by doping silver nanowires. *Sensors* **2014**, *14*, 9889−9899.
(23) Park, S. H.; Lee, H. B.; Yeon, S. M.; Park, J.; Lee, N. K. Flexible and stretchable piezoelectric sensor with thickness-tunable configuration of electrospun nanofiber mat and elastomeric substrates. *ACS Appl. Mater. Interfaces* **2016**, *8*, 24773−24781.
(24) Gheibi, A.; Bagherzadeh, R.; Merati, A. A.; Latifi, M. Electrical power generation from piezoelectric electrospun nanofibers membranes: electrospinning parameters optimization and effect of membranes thickness on output electrical voltage. *J. Polym. Res.* **2014**, *21*, 571.
(25) Baji, A.; Mai, Y. W.; Li, Q.; Liu, Y. Electrospinning induced ferroelectricity in poly (vinylidene fluoride) fibers. *Nanoscale* **2011**, *3*, 3068−3071.
(26) Parangusan, H.; Ponnamma, D.; Al-Maadeed, M. A. Stretchable electrospun PVDF-HFP/Co-ZnO nanofibers as piezoelectric nanogenerators. *Sci. Rep.* **2018**, *8*, No. 754.
(27) Parangusan, H.; Ponnamma, D.; AlMaadeed, M. A. Flexible trilayer piezoelectric nanogenerator based on PVDF-HFP/Ni-doped ZnO nanocomposites. *RSC Adv.* **2017**, *7*, 50156−50165.
(28) Harish, K. N.; Bhojya Naik, H. S.; Prashanth Kumar, P. N.; Viswanath, R. Optical and photocatalytic properties of solar light active Nd-substituted Ni ferrite catalysts: for environmental protection. *ACS Sustainable Chem. Eng.* **2013**, *1*, 1143−1153.
(29) Etacheri, V.; Roshan, R.; Kumar, V. Mg-doped ZnO nanoparticles for efficient sunlight-driven photocatalysis. *ACS Appl. Mater. Interfaces* **2012**, *4*, 2717−2725.
(30) Liang, X.; Hu, S.; Shen, S. Size-dependent buckling and vibration behaviors of piezoelectric nanostructures due to flexoelectricity. *Smart Mater. Struct.* **2015**, *24*, No. 105012.
(31) Martins, P.; Lopes, A. C.; Lanceros-Mendez, S. Electroactive phases of poly (vinylidene fluoride): determination, processing and applications. *Prog. Polym. Sci.* **2014**, *39*, 683−706.
(32) Abbrent, S.; Plestil, J.; Hlavata, D.; Lindgren, J.; Tegenfeldt, J.; Wendsjö, Å. Crystallinity and morphology of PVdF−HFP-based gel electrolytes. *Polymer* **2001**, *42*, 1407−1416.
(33) Adhikary, P.; Garain, S.; Ram, S.; Mandal, D. Flexible hybrid eu3+ doped P (VDF-HFP) nanocomposite film possess hypersensitive electronic transitions and piezoelectric throughput. *J. Polym. Sci., Part B: Polym. Phys.* **2016**, *54*, 2335−2345.
(34) Kanik, M.; Aktas, O.; Sen, H. S.; Durgun, E.; Bayindir, M. Spontaneous high piezoelectricity in poly (vinylidene fluoride) nanoribbons produced by iterative thermal size reduction technique. *ACS Nano* **2014**, *8*, 9311−9323.
(35) Kar, E.; Bose, N.; Das, S.; Mukherjee, N.; Mukherjee, S. Enhancement of electroactive $\beta$ phase crystallization and dielectric constant of PVDF by incorporating $GeO_2$ and $SiO_2$ nanoparticles. *Phys. Chem. Chem. Phys.* **2015**, *17*, 22784−22798.
(36) Zhang, Y. Y.; Jiang, S. L.; Yu, Y.; Xiong, G.; Zhang, Q. F.; Guang, G. Z. Phase transformation mechanisms and piezoelectric properties of poly (vinylidene fluoride)/montmorillonite composite. *J. Appl. Polym. Sci.* **2012**, *123*, 2595−2600.
(37) Benz, M.; Euler, W. B. Determination of the crystalline phases of poly (vinylidene fluoride) under different preparation conditions using differential scanning calorimetry and infrared spectroscopy. *J. Appl. Polym. Sci.* **2003**, *89*, 1093−1100.
(38) Garain, S.; Jana, S.; Sinha, T. K.; Mandal, D. Design of in situ poled Ce3+-doped electrospun PVDF/graphene composite nanofibers for fabrication of nanopressure sensor and ultrasensitive acoustic nanogenerator. *ACS Appl. Mater. Interfaces* **2016**, *8*, 4532−4540.
(39) Tamang, A.; Ghosh, S. K.; Garain, S.; Alam, M. M.; Haeberle, J.; Henkel, K.; Schmeisser, D.; Mandal, D. DNA-assisted $\beta$-phase nucleation and alignment of molecular dipoles in pvdf film: a realization of self-poled bioinspired flexible polymer nanogenerator for portable electronic devices. *ACS Appl. Mater. Interfaces* **2015**, *7*, 16143−16147.
(40) Adhikary, P.; Mandal, D. Enhanced electro-active phase in a luminescent P (VDF−HFP)/Zn 2+ flexible composite film for piezoelectric based energy harvesting applications and self-powered UV light detection. *Phys. Chem. Chem. Phys.* **2017**, *19*, 17789−17798.
(41) Liu, X.; Ma, J.; Wu, X.; Lin, L.; Wang, X. Polymeric nanofibers with ultrahigh piezoelectricity via self-orientation of nanocrystals. *ACS Nano* **2017**, *11*, 1901−1910.
(42) Mandal, D.; Henkel, K.; Schmeißer, D. Improved performance of a polymer nanogenerator based on silver nanoparticles doped electrospun P(VDF−HFP) nanofibers. *Phys. Chem. Chem. Phys.* **2014**, *16*, 10403−10407.
(43) Zeng, W.; Tao, X. M.; Chen, S.; Shang, S.; Chan, H. L.; Choy, S. H. Highly durable all-fiber nanogenerator for mechanical energy harvesting. *Energy Environ. Sci.* **2013**, *6*, 2631−2638.
(44) Ponnamma, D.; Poornima, V. P.; Al-Maadeed, M. A. 3D architectures of titania nanotubes and graphene with efficient nanosynergy for supercapacitors. *Mater. Des.* **2017**, *117*, 203−212.
(45) Liu, F.; Hashim, N. A.; Liu, Y.; Abed, M. M.; Li, K. Progress in the production and modification of PVDF membranes. *J. Membr. Sci.* **2011**, *375*, 1−27.
(46) Senthilkumar, N.; Babu, K. J.; Gnana kumar, G.; Kim, A. R.; Yoo, D. J. Flexible electrospun PVdF-HFP/Ni/Co membranes for efficient and highly selective enzyme free glucose detection. *Ind. Eng. Chem. Res.* **2014**, *53*, 10347−10357.
(47) Hirsh, S. L.; Nosworthy, N. J.; Kondyurin, A.; Dos Remedios, C. G.; McKenzie, D. R.; Bilek, M. M. Linker-free covalent thermophilic $\beta$-glucosidase functionalized polymeric surfaces. *J. Mater. Chem.* **2011**, *21*, 17832−17841.
(48) Shah, D.; Maiti, P.; Gunn, E.; Schmidt, D. F.; Jiang, D. D.; Batt, C. A.; Giannelis, E. P. Dramatic enhancements in toughness of polyvinylidene fluoride nanocomposites via nanoclay-directed crystal structure and morphology. *Adv. Mater.* **2004**, *16*, 1173−1177.
(49) He, F. A.; Lin, K.; Shi, D. L.; Wu, H. J.; Huang, H. K.; Chen, J. J.; Chen, F.; Lam, K. H. Preparation of organosilicate/PVDF composites with enhanced piezoelectricity and pyroelectricity by stretching. *Compos. Sci. Technol.* **2016**, *137*, 138−147.
(50) Liang, C. L.; Mai, Z. H.; Xie, Q.; Bao, R. Y.; Yang, W.; Xie, B. H.; Yang, M. B. Induced Formation of Dominating Polar Phases of Poly (vinylidene fluoride): Positive Ion−CF2 Dipole or Negative Ion−CH2 Dipole Interaction. *J. Phys. Chem. B* **2014**, *118*, 9104−9111.
(51) Mandal, A.; Nandi, A. K. Ionic liquid integrated multiwalled carbon nanotube in a poly (vinylidene fluoride) matrix: formation of a piezoelectric $\beta$-polymorph with significant reinforcement and


DOI: 10.1021/acsomega.9b00243
*ACS Omega* 2019, 4, 6312−6323

conductivity improvement. *ACS Appl. Mater. Interfaces* **2013**, *5*, 747−760.
(52) Khalifa, M.; Mahendran, A.; Anandhan, S. Probing the synergism of halloysite nanotubes and electrospinning on crystallinity, polymorphism and piezoelectric performance of poly (vinylidene fluoride). *RSC Adv.* **2016**, *6*, 114052−114060.
(53) Aepuru, R.; Rao, B. B.; Kale, S. N.; Panda, H. S. Unique negative permittivity of the pseudo conducting radial zinc oxide-poly (vinylidene fluoride) nanocomposite film: Enhanced dielectric and electromagnetic interference shielding properties. *Mater. Chem. Phys.* **2015**, *167*, 61−69.
(54) Deshmukh, K.; Ahamed, M. B.; Deshmukh, R. R.; Pasha, S. K.; Sadasivuni, K. K.; Polu, A. R.; Ponnamma, D.; AlMaadeed, M. A.; Chidambaram, K. Newly developed biodegradable polymer nanocomposites of cellulose acetate and Al2O3 nanoparticles with enhanced dielectric performance for embedded passive applications. *J. Mater. Sci.: Mater. Electron.* **2017**, *28*, 973−986.
(55) Deshmukh, K.; Ahamed, M. B.; Sadasivuni, K. K.; Ponnamma, D.; AlMaadeed, M. A.; Deshmukh, R. R.; Pasha, S. K.; Polu, A. R.; Chidambaram, K. Fumed SiO2 nanoparticle reinforced biopolymer blend nanocomposites with high dielectric constant and low dielectric loss for flexible organic electronics. *J. Appl. Polym. Sci.* **2017**, *134* (5), 44427.
(56) Paria, S.; Karan, S. K.; Bera, R.; Das, A. K.; Maitra, A.; Khatua, B. B. A facile approach to develop a highly stretchable PVC/ZnSnO3 piezoelectric nanogenerator with high output power generation for powering portable electronic devices. *Ind. Eng. Chem. Res.* **2016**, *55*, 10671−10680.
(57) Thakur, P.; Kool, A.; Bagchi, B.; Das, S.; Nandy, P. Effect of in situ synthesized Fe 2 O 3 and Co3O4 nanoparticles on electroactive $\beta$ phase crystallization and dielectric properties of poly (vinylidene fluoride) thin films. *Phys. Chem. Chem. Phys.* **2015**, *17*, 1368−1378.
(58) Chinya, I.; Pal, A.; Sen, S. Polyglycolated zinc ferrite incorporated poly (vinylidene fluoride)(PVDF) composites with enhanced piezoelectric response. *J. Alloys Compd.* **2017**, *722*, 829−838.
(59) Kim, H. J.; Kim, J. H.; Jun, K. W.; Kim, J. H.; Seung, W. C.; Kwon, O. H.; Park, J. Y.; Kim, S. W.; Oh, I. K. Silk nanofiber-networked bio-triboelectric generator: Silk Bio-TEG. *Adv. Energy Mater.* **2016**, *6*, No. 1502329.
(60) Alam, M. M.; Ghosh, S. K.; Sultana, A.; Mandal, D. Lead-free ZnSnO3/MWCNTs-based self-poled flexible hybrid nanogenerator for piezoelectric power generation. *Nanotechnology* **2015**, *26*, No. 165403.
(61) Bakar, E. A.; Mohamed, M. A.; Ooi, P. C.; Wee, M. M.; Dee, C. F.; Majlis, B. Y. Fabrication of indium-tin-oxide free, all-solution-processed flexible nanogenerator device using nanocomposite of barium titanate and graphene quantum dots in polyvinylidene fluoride polymer matrix. *Org. Electron.* **2018**, *61*, 289−295.



DOI: 10.1021/acsomega.9b00243
*ACS Omega* 2019, 4, 6312−6323